Modeling rhythmic patterns in the hippocampus

A. I. Lavrova[*]
Institute of Physics, Humboldt-University at Berlin, Newtonstrasse 15, 12489 Berlin, Germany

M. A. Zaks[†]
Institute of Mathematics, Humboldt-University at Berlin, Rudower Chaussee 25, 12489 Berlin, Germany

L. Schimansky-Geier[‡]
Institute of Physics, Humboldt-University at Berlin, Newtonstrasse 15, 12489 Berlin, Germany

(Received 11 November 2011; revised manuscript received 10 February 2012; published 27 April 2012)

We investigate different dynamical regimes of the neuronal network in the CA3 area of the hippocampus. The proposed neuronal circuit includes two fast- and two slowly spiking cells which are interconnected by means of dynamical synapses. On the individual level, each neuron is modeled by FitzHugh-Nagumo equations. Three basic rhythmic patterns are observed: the gamma rhythm in which the fast neurons are uniformly spiking, the theta rhythm in which the individual spikes are separated by quiet epochs, and the theta-gamma rhythm with repeated patches of spikes. We analyze the influence of asymmetry of synaptic strengths on the synchronization in the network and demonstrate that strong asymmetry reduces the variety of available dynamical states. The model network exhibits multistability; this results in the occurrence of hysteresis in dependence on the conductances of individual connections. We show that switching between different rhythmic patterns in the network depends on the degree of synchronization between the slow cells.

DOI: 10.1103/PhysRevE.85.041922 PACS number(s): 87.18.Sn, 87.19.ll

I. INTRODUCTION

Rhythmic behavior is a basic property of biological systems and plays an important role in a variety of physiological processes [1]. In particular, hippocampal neurons of the human brain are able to generate rhythmic oscillations in several frequency ranges; among these, prominent roles belong to fast (gamma rhythm, 30–65 Hz) and slow (theta rhythm, 3–10 Hz) signals and to mixed regimes in which fast and slow oscillations alternate. The theta rhythm has been demonstrated to be responsible for coding of spatial information [2] and synaptic modification of intrahippocampal pathways, as well as for assembling and segregation of neuronal groups [3]. In its turn, oscillatory activity in the gamma-frequency band is involved in information transmission and storage [4]. Isolated parts (so-called CA1, CA3, DG, etc.) of hippocampal formation where these regimes are observed have been subjected to numerous experiments [5–10]. In particular, it has been established that the neuronal network in the CA3 region of the hippocampus can exhibit three qualitatively different oscillatory states (theta, gamma, and the mixed "theta-gamma") and is able to dynamically switch between them [7]. Transitions between different regimes in brain neuronal networks can be provoked not only by variation of parameters, but by variation of initial conditions as well [11–14]; the latter may occur due to changes in the baseline potential [13] or to perturbations of initial ionic concentrations [15].

The cells that constitute a hippocampal network differ in their morphological, electrophysiological, and neurochemical properties [16]. Synaptic interactions between several types of cells [the pyramidal, basket, septum, and oriens-lacunosum-moleculare (OLM) cells] are responsible for the generation of different rhythms [10].

Besides experimental studies, transitions between various rhythms and multistability phenomena in isolated cells as well as in neuronal networks have been subjected to theoretical and numerical modeling [7,17–20]. Typically, such models involve various cell types as well as large numbers of ionic currents and compartments. In the detailed models [19,21] as well as in simpler biophysical approximations [17] the cells responsible for the generation of rhythmic patterns are typically described by equations of the Hodgkin-Huxley type.

The role of intercellular synchronization in the transitional processes is an object of ongoing discussions. In particular, it has been shown [22] that a switching between two states of the system can forecast desynchronization in a bursting activity of the hippocampus. The strength of intercellular coupling governed by synaptic conductances is apparently a crucial factor in this context [7,23]. For example, studies of a detailed thalamocortical model [20] have shown that the presence or absence of bistability in the neuronal circuit can depend on parameters of the electrical coupling between neurons as well as on the synaptic conductance.

The obligatory in realistic models high degree of complexity hampers the revelation of the principal mechanisms and control parameters of transitions between different types of oscillation. Therefore, along with an accurate reproduction of experimental observations, one of the main aims of the modeling remains the consideration of general dynamics in the appropriate class of circuits, as well as an understanding of the underlying dynamical mechanisms which are responsible for different rhythmic patterns. This raises a question about the minimal module of the hippocampal network: a small set of cells capable of reproducing all basic typs of experimentally observable rhythms [17]. Embedded into intricate networks of

[*]aurebours@googlemail.com
[†]zaks@math.hu-berlin.de
[‡]alsg@physik.hu-berlin.de

neurons, such modules can play the role of pacemakers which ensure persistence of optimal oscillatory states in the entire ensemble.

Below we discuss a minimalistic dynamical model of the hippocampal circuit in the area CA3, which is able to produce several rhythmic patterns. For this purpose we simplify the basic module of the circuit in such a way that maintenance of the essential types of dynamical regimes is controlled by a concise number of principal parameters. Since we do not aim at detailed reproduction of the intrinsic cellular dynamics but restrict ourselves to rhythmic aspects, we reduce the description of each element to the classical simplified model of neuronal oscillations: the FitzHugh-Nagumo (FHN) equations. The simplification of the elements in this case does not imply trivialization of the dynamics: ensembles of FHN oscillators are known to exhibit different kinds of collective behavior which, depending on the topology and strength of interaction, range from subthreshold oscillations via mixed-mode intermittency to tonic spiking [24]. Interplay between the connectivity and coupling strength in networks of heterogeneous FHN oscillators can induce or destroy synchrony [25]. Working with FHN neurons ensures the well understood dynamics on the level of individual elements, and allows us to concentrate on the governing role of interactions between them.

In Sec. II we introduce the model equations and discuss the choice of appropriate parameter values. Section III begins with characterization of the principal rhythmic patterns; in particular, the role of the phase shift between the OLM cells is discussed. Further, we proceed to the description of multistability and transitions between the patterns. We demonstrate that the model reproduces the basic rhythms observed experimentally, as well as hysteresis between them. Finally, we show how the symmetry or asymmetry in the arrangement of synaptic connections influences the existence and properties of dynamical states.

II. MODEL EQUATIONS

In a recent paper [7], a kind of minimalistic network for studies of different regimes in the hippocampal area CA3 has been proposed. This network includes the main types of hippocampal cells and consists of five elements: two fast-oscillating cells (so-called basket cells), two slow cells (OLM-associated cells), and one two-compartmental pyramidal cell. The cells are synaptically connected in all-to-all topology, with one exception: there is no direct connection between the slowly spiking cells. Accordingly, the pyramidal cell activates the rest of the cells which, in turn, inhibit each other and the pyramidal cell. The cells are described within the framework of the Hodgkin-Huxley formalism. After taking into account all relevant currents as well as the kinetics of synaptic variables, the resulting system constitutes a set of 41 ordinary differential equations. Notably, the choice of coupling coefficients employed in Ref. [7] ensured a certain degree of asymmetry in the network: in particular, each basket cell was coupled to both OLM cells through connections with different conductivities.

Numerical simulations of that model have confirmed that transitions between different regimes depend on the strength

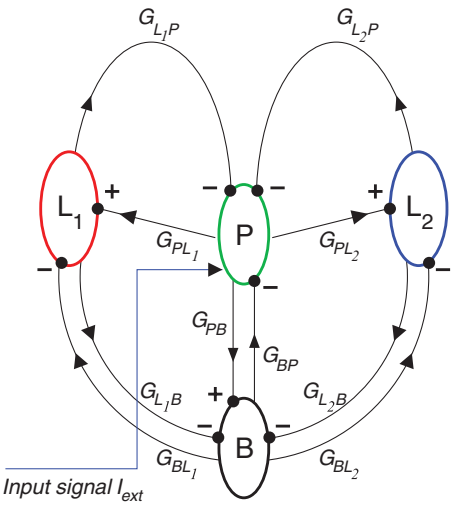

FIG. 1. (Color online) Sketch of the cellular network. $L_{1,2}$, slow OLM cells; P, fast pyramidal cell; B, basket cell. Arrows, directions of currents; filled circles, synapses; pluses, excitatory synapses; minuses, inhibitory synapses. Synaptic connections are characterized by conductances G_{ji}. External input I_{ext} affects only the pyramidal cell P.

of coupling between the cells. Typically, a switching between different rhythms is preceded by the onset of a certain phase shift between two slow-spiking cells. Within the model of [7], this shift can be ensured, e.g., by a judicious choice of appropriate initial conditions.

In the present work we further reduce the complexity of the model: we decrease the number of cells and replace the Hodgkin-Huxley setup by the FitzHugh-Nagumo equations. The resulting network, sketched in Fig. 1, includes a one-compartmental pyramidal cell P, one basket cell B, and two OLM cells L_1 and L_2. All cells are mutually synaptically connected; the only exceptions are the two slow OLM cells which do not communicate directly. Synaptic connections are governed by the synaptic conductances G_{ji} with $j,i = L_1, L_2, P, B$ (and $G_{jj} = 0$). Leaving in the network only one basket cell B, we take into account, however, inequality of the cross and direct connections as a potential source of a phase shift between the slowly spiking cells. For this purpose, it is sufficient to allow for asymmetric synaptic inputs from the basket cell to L_1 and L_2: in general, $G_{BL_1} \neq G_{BL_2}$. The rest of the connections are set symmetrically: $G_{PL_1} = G_{PL_2} = G_{PL}$, $G_{L_1P} = G_{L_2P} = G_{LP}$, $G_{L_1B} = G_{L_2B} = G_{LB}$.

Within this simplified description, it appears reasonable to keep only one activating input which acts upon the fast-oscillating cell P. The latter excites all other cells, which inhibit each other as well as P itself.

We use below the form of equations in which all variables and, hence, all parameters are measured in dimensionless units. Each cell of the network obeys the standard set of coupled FitzHugh-Nagumo equations:

$$\begin{aligned} \frac{dv_i}{dt} &= v_i - \frac{v_i^3}{3} - u_i + I_{\text{ext}}\delta_{i,P} + \sum_j I_{\text{syn}}^{(ji)}, \\ \frac{du_i}{dt} &= \varepsilon_i\,(v_i + a - b\,u_i), \end{aligned} \tag{1}$$

where v_i is the membrane potential of the ith cell (recall that $i = L_1, L_2, P, B$), and u_i is the corresponding membrane variable. The values of the parameters a and b are the same for all cells. The Kronecker delta $\delta_{i,P}$ ensures that only the pyramidal cell is externally excited by the current I_{ext}.

The synaptic input $I_{\text{syn}}^{(ji)}$ in Eqs. (1)—the current from cell j to cell i—is defined as

$$I_{\text{syn}}^{(ji)} = G_{ji} s_{ji} (E_{\text{ex,in}} - v_i)$$

and is governed by the kinetic equation for the synaptic variable $s_{ji}(t)$ [17]:

$$\frac{ds_{ji}}{dt} = \frac{A}{2}\left(1 + \tanh\frac{v_j}{v_{vsl}}\right)(1 - s_{ji}) - B s_{ji}. \qquad (2)$$

For simplicity, we assume that all synapses obey quantitatively the same kinetics. This is achieved by using the same values of A, B, and v_{vsl} in Eq. (2) for all s_{ji}. Hence, evolution of s_{ji} depends (via v_j) only on j, and the number of independent synaptic variables equals the number of cells in the network. Altogether, the dynamical system includes 12 ordinary differential equations: eight equations for the FitzHugh-Nagumo variables along with four equations for the synaptic variables.

Originally, the FitzHugh-Nagumo equations were written as a crude simplistic model which mimics the characteristic features of the Hodgkin-Huxley dynamics. Hence, their parameters do not allow for direct biological interpretation and serve the mere purpose of supporting the proper dynamical regimes. To illustrate possible kinds of dynamics in the considered network, we fix the parameters of the FitzHugh-Nagumo equations (1) at the values which ensure that in the absence of external currents every isolated cell is at rest; if perturbed by sufficient external input, it displays full-scale oscillations. The values $a = 0.5$, $b = 0.8$ which we use for our calculations are close to those employed by FitzHugh [26].

The parameter ε_i in the FitzHugh-Nagumo equations (1) determines the time scale of oscillations in the isolated ith cell: in the leading order, the period of relaxation oscillations in a cell is inversely proportional to ε_i. The dimensionless number ε_i can be interpreted as the ratio of two *dimensional* time scales of the neuron: that of the fastest relaxation to that of the slowest one. In the case of the pyramidal and basket cells these are the relaxation times of, respectively, potassium and sodium currents; the values of ε_i for these two cells can be viewed as (approximately) the same. In contrast, in the OLM cells the slowest processes involve relaxation of specific so-called hyperpolarization-activated currents [8,27], and their values of ε_i should be chosen substantially lower. Accordingly, we set $\varepsilon = 0.3$ for the fast basket and pyramidal cells, whereas for slow L cells the value $\varepsilon = 0.04$ is adopted.

Equation (2) for synaptic variables are phenomenological as well; the values of the parameters A, B, and v_{vsl} are commonly obtained by fitting the experimentally measured dependencies. By setting $A = 1$, $B = 0.3$, and $v_{vsl} = 0.1$ we model the typical situation in which opening of channels occurs faster—but not much faster—than their subsequent closure.

The value of E in the expression for the synaptic current depends on the kind of connection. For all excitatory synapses we put $E_{\text{ex}} = 0$, whereas for inhibitory synapses $E_{\text{in}} = -5$ is set. The latter value ensures that the difference $E_{\text{in}} - v_i$, and thereby the corresponding synaptic current $I_{\text{syn}}^{(ji)}$, stay negative at all times, and the connection is indeed inhibitory.

Concerning the synaptic conductances G_{ji}, we choose values which, dimensionalized in units of 0.01 Ω^{-1} m^{-2}, have the order of magnitude of those reported in Ref. [7]. In a sense, the conductances predetermine the relative importance of individual cells in the ensemble. Since the external current acts only upon the pyramidal cell, synaptic connections from this cell to the rest of the module should be strong enough to activate the otherwise silent basket and OLM cells; this is ensured by assigning to them relatively high values $G_{PL} = 0.7$ and $G_{PB} = 0.57$. A lower conductivity is assigned to the backward connection from the basket to the pyramidal cell: $G_{BP} = 0.1$. Further, we introduce *asymmetry* between the left and right halves of the network by fixing different values for connections from the basket to the OLM cells: $G_{BL_1} = 0.06$ in contrast to $G_{BL_2} = 0.03$.

The slow OLM cells are driven by the pyramidal cell; the intensity of their inhibitory feedback to the driving element depends on the conductances G_{LP} and (mediated by the basket cell) on the conductances G_{LB}. If both G_{LB} and G_{LP} are set to zero, the feedback is absent, and the OLM cells play a passive role. Each of them oscillates periodically; the OLM cell is phase locked to the oscillations of the driving fast subsystem formed by the pyramidal cell and the basket cell. However, due to asymmetry, the slow cells can be locked (and under the quoted parameter values are indeed locked) to the fast subsystem in different locking ratios. Asymmetry of the rhythmic patterns persists for sufficiently low values of G_{LB} and G_{LP}: this is visualized in the lower panel of Fig. 2 where the slow cells oscillate in the ratio 2:3. An increase of the conductances G_{LB} and/or G_{LP} intensifies the feedback; in spite of the absence of a direct connection, the OLM cells interact through the mediation of the fast cells, and their periods get adjusted.

In order to concentrate on the role of connection from the OLM cells to the pyramidal cell, we use throughout this work

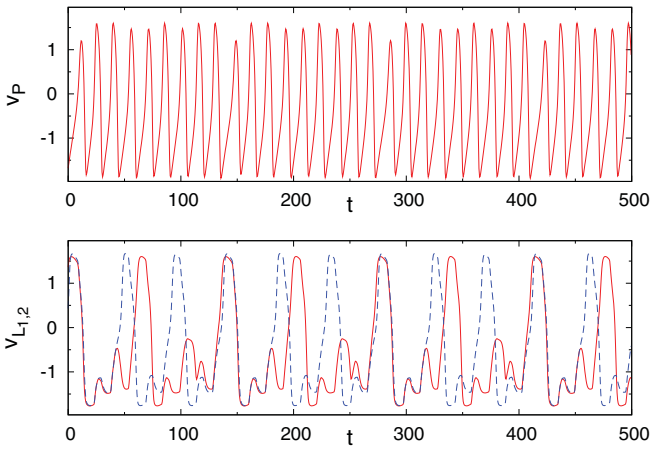

FIG. 2. (Color online) Gamma rhythm at $G_{LP} = 0.032$, $G_{LB} = 0.001$. Top: pyramidal cell; periodic pattern which consists of nine spikes. Bottom: OLM cells; solid curve, L_1; dashed curve, L_2. OLM cells are locked in the frequency ratio 2:3.

the conductance G_{LP} as a controlling parameter and study transitions which occur in the course of its variation. As for the connection from the OLM to the basket cell, it should be weak enough not to damp the module dynamics; hence we fix for our calculations (with the only exception of the plot in Fig. 2) the value $G_{LB} = 0.01$. This value is sufficiently high to ensure that the feedback via the basket cell synchronizes the slow cells in the frequency ratio 1:1, even in the absence of direct feedback through the LP connections.

The steady-state solution of the equations corresponds to the quiescent nonspiking state. The intensity of the constant external input I_{ext} (recall that it affects only the P cell) should ensure destabilization of the equilibrium and sustenance of oscillations in the system. Under $G_{LP} = 0.037$ and the aforementioned fixed values of the other parameters, the equilibrium is unstable for $0.02 < I_{\text{ext}} < 1.1$. At the endpoints of this interval, subcritical Hopf bifurcations take place. The location of the endpoints is almost insensitive to variation of G_{LP}. Accordingly, for our numerical simulations we take the value of the input from this range: $I_{\text{ext}} = 0.43$.

Numerical solutions have been obtained using the software packages XPPAUT and MATCONT.

III. RESULTS

In order to characterize different attractors of the system and to understand possible mechanisms of switching between the regimes, we have studied the response of the model to variation of the strength of the LP connection. Starting from the situation when this connection is absent, we describe below the states which are observed in the course of increase of G_{LP}.

Among the solutions, we single out three main qualitative types of oscillation. The difference between them lies in the behavior of the voltage variables of fast (pyramidal or basket) neurons: In the gamma rhythm the voltage exhibits fast regular oscillations, whose amplitude is weakly modulated due to interaction with slow counterparts. In the theta-gamma rhythm certain spikes in the pattern "fall out"; the plot shows regular patches of spikes interrupted by nearly quiescent epochs. Typically, theta-gamma oscillations are periodic. Finally, the theta pattern consists of repeated solitary spikes on the nearly quiescent background. For a slow OLM cell the difference in the temporal dynamics between the three rhythms is not so pronounced; here, transitions manifest themselves in the onset or the disappearance of a phase shift between two such cells.

A. Gamma rhythm

If the value of the conductance G_{LP} is set to zero, the OLM cells exert no inhibiting action upon the pyramidal cell; this corresponds to removal of the upper connecting arcs in the scheme of Fig. 1. In this situation, the system performs periodic oscillations of the gamma type. Consecutive spikes in the fast cells occur at close time intervals, but the exact repetition (in other words, closure of the limit cycle in the phase space of the system) requires several spikes. In particular, smallness of G_{LB} can result in asynchrony between the slow cells (Fig. 2).

By continuity, rhythmic pattern of the gamma type persists at sufficiently low nonzero values of G_{LP} as well. An example

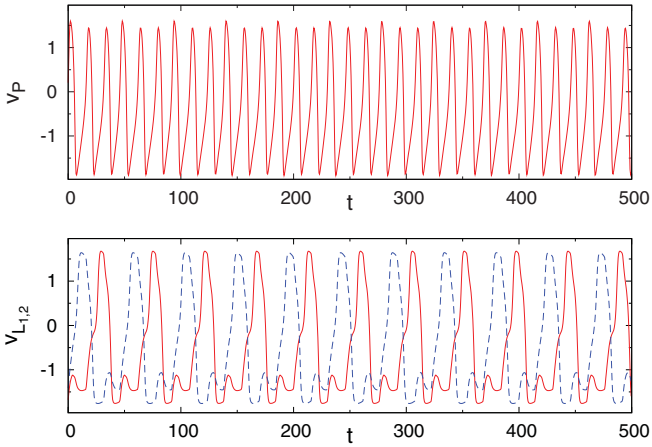

FIG. 3. (Color online) Gamma rhythm at $G_{LP} = 0.035$, $G_{LB} = 0.01$. Top: pyramidal cell. Bottom: OLM cells; solid curve, L_1; dashed curve, L_2. OLM cells are locked in a 1:1 ratio; note the phase shift between them.

is shown in Fig. 3. At $G_{LP} = 0.035$ the slow cells oscillate in the ratio 1:1 (bottom panel), but their maxima do not occur simultaneously. In this context it is natural to speak about the phase shift. We introduce the phase phenomenologically: for each cell the phase increment of 2π is assigned to every interval between two consecutive positive maxima of voltage; between the maxima, the phase is linearly interpolated. The phase shift between oscillations shown in the bottom panel of Fig. 3 is close to $2\pi/3$.

B. Theta-gamma rhythm

In a broad range of values of G_{LP} above 0.0362 an appropriate choice of initial condition results in a different rhythmic pattern: the system exhibits theta-gamma oscillations. The bottom panel of Fig. 4 indicates that in the theta-gamma state both slow cells oscillate synchronously; there is no phase shift between them.

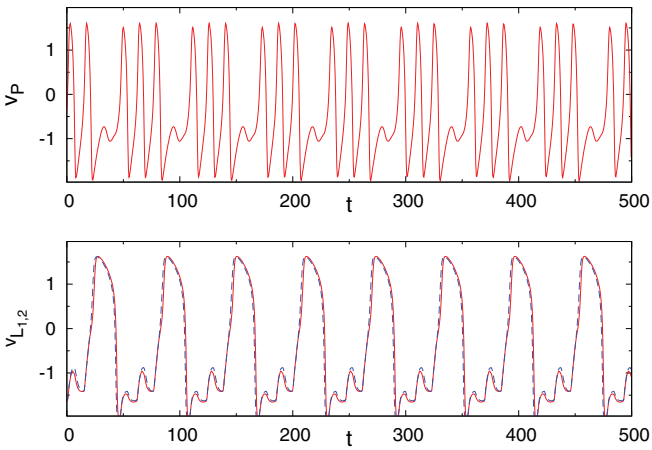

FIG. 4. (Color online) Theta-gamma rhythm close to its onset; $G_{LP} = 0.05$. Top: pyramidal cell. Bottom: OLM cells; solid curve, L_1; dashed curve, L_2.

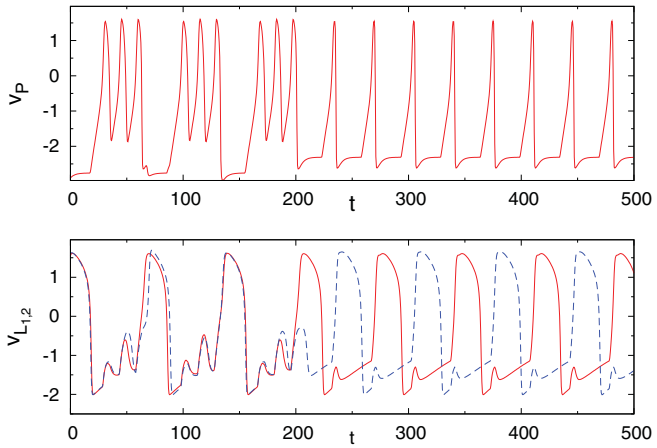

FIG. 5. (Color online) Breakdown of theta-gamma rhythm and onset of theta rhythm; $G_{LP} = 2.274$. Top: pyramidal cell. Bottom: OLM cells; solid curve, L_1; dashed curve, L_2. Note the in-phase oscillations before the switch and antiphase immediately after it.

C. Theta rhythm

At sufficiently high values of G_{LP} the theta-gamma rhythm is replaced by theta oscillations. Switching between the two regimes is visualized in Fig. 5: the motion starts as a typical theta-gamma oscillation, with patches of spikes of the fast cell; in the course of time evolution, at around $t \approx 200$, it abruptly changes the pattern and acquires the characteristic shape of the theta rhythm with equidistant solitary spikes of the fast cell. Remarkably, the slow cells, synchronous in the initial stage, develop during the switch a phase shift of π: in the theta rhythm the OLM cells oscillate in antiphase.

D. Hysteresis

Over large intervals of values of G_{LP}, different rhythmic patterns coexist as attractors of Eqs. (1) and (2): at low values of G_{LP}, depending on the initial values of the variables, the system can exhibit gamma as well as theta-gamma oscillations, whereas at moderate and high values of G_{LP} there is a hysteresis between theta-gamma and pure theta patterns.

For slow OLM cells, neither a transition between gamma and theta-gamma states nor the further growth of G_{LP} significantly affects the period of their oscillations. In contrast, the periodicity in spiking patterns of the fast cells P and B changes quite noticeably. A convenient characteristic is delivered by the average duration of the interspike interval (ISI): the mean distance between positive maxima of voltage in a cell. In Fig. 6, we plot this characteristic for membrane potential oscillations in the pyramidal cell. The value of the ISI increases from 14.73 in the gamma state at $G_{LP} = 0$ to 35.94 in the theta state at $G_{LP} = 3$. A similar situation is observed for the basket cell.

A closer look shows that gamma and theta branches are connected; in fact, they belong to the same continuous family of solutions. A transformation from the gamma to the theta rhythm occurs through the intermediate regime which is observed within the small parameter range $0.0724 < G_{LP} < 0.0734$. The main stages of this process, in terms of the voltage variable of the pyramidal cell, are presented in Fig. 7.

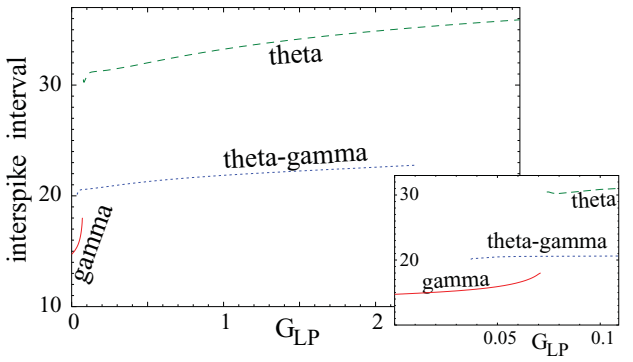

FIG. 6. (Color online) Duration of interspike intervals in dependence on G_{LP} for different rhythmic patterns. Solid line, gamma rhythm; dotted line, theta-gamma pattern; dashed line, theta rhythm. Inset: range of low values of the conductance G_{LP}.

The transformation is preceded by a gradual deformation of the gamma pattern: of the three initially nearly equal spikes (see Fig. 3), two spikes get diminished [Figs. 7(a) and 7(b)]. As a result, the periodic gamma state acquires the characteristic shape of mixed-mode oscillations [28] with alternating small subthreshold and large-scale spiking maxima. At $G_{LP} = 0.0726$ these oscillations form the complicated (yet periodic, with period 541.1) temporal pattern visualized in Fig. 7(c). A small increase of G_{LP} leads to partial flattening of subthreshold epochs [Fig. 7(d)]; the next small increment results in the regular alternation of a spike and a single subthreshold oscillation [Fig. 7(e)]. In fact, this state is already very close to the theta pattern; further increase of G_{LP} brings only quantitative changes: the subthreshold oscillations are gradually flattened and eliminated, and the theta state is established. On the phase portrait (Fig. 8), the epochs of subthreshold oscillations are represented by minor loops of the trajectory. In the course of flattening, these loops get smaller, turn into cusps, and disappear, so that only the large loops (corresponding to solitary spikes of the theta rhythm) persist.

Remarkably, the described transformation changes the phase difference between the slow cells: as already mentioned, in the gamma state the difference is close to $2\pi/3$, and the proximity to this value holds until the onset of mixed-mode oscillations in Fig. 7(c). As soon as the simple temporal pattern is regained [Fig. 7(e)] the phase difference acquires a value close to π, and the antiphase oscillations of slow cells remain the hallmark of the theta state everywhere in the range of its existence.

A similar process of deformation occurs on the other branch of solutions, which corresponds to the theta-gamma state. In this state, patches of full-scale spikes are separated by subthreshold oscillations (see Fig. 4); the latter correspond to minor loops on the projections of the respective phase portraits. In the course of increase of the conductance G_{LP}, the shape of the attracting orbit is subjected to continuous deformation (similarly to that shown in Fig. 8 for the theta rhythm): the minor loop gradually gets smaller, shrinks into a cusp, and disappears completely. This process leads to gradual decrease and elimination of one of the maxima in the temporal pattern of the oscillations.

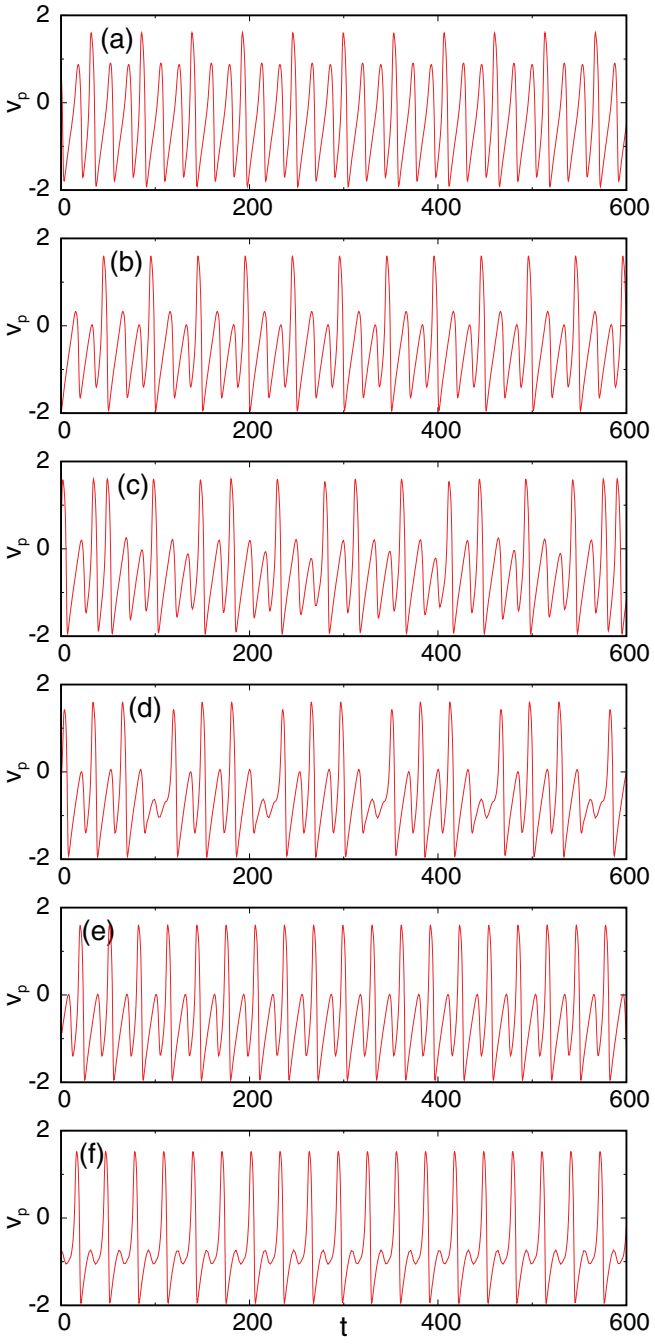

FIG. 7. (Color online) Transformation of the gamma into the theta rhythm for the membrane voltage of the pyramidal cell. (a) $G_{LP} = 0.07$; (b) $G_{LP} = 0.0724$; (c) $G_{LP} = 0.0726$; (d) $G_{LP} = 0.0732$; (e) $G_{LP} = 0.0734$; (f) $G_{LP} = 0.1000$.

As seen in Fig. 6, the branch of theta-gamma oscillations is isolated in the parameter space. A closer look shows that its creation at low values of G_{LP} begins with a very short segment of mixed-mode oscillations; they are present close to $G_{LP} = 0.0362$, but already at $G_{LP} = 0.0363$ the characteristic shape of periodic theta-gamma oscillations is established. On the other end of the branch, at $G_{LP} = 2.274$, the limit cycle which corresponds to the theta-gamma rhythmic pattern disappears in the saddle-node bifurcation.

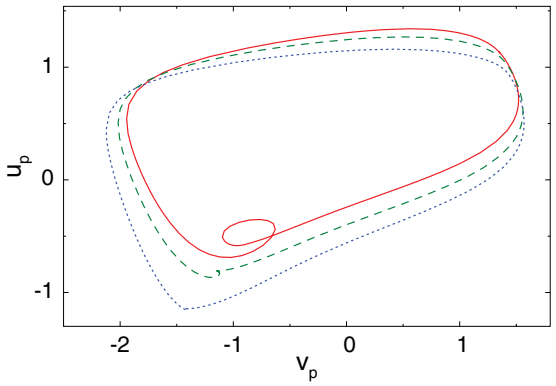

FIG. 8. (Color online) Evolution in the phase space of the attractor shape in the theta rhythm; projection on the variables of the pyramidal cell. Minor loops, which correspond to subthreshold oscillations, shrink, turn into cusps, and disappear. Solid line, $G_{LP} = 0.09$; dashed line, $G_{LP} = 0.2$; dotted line, $G_{LP} = 0.4$.

E. Attraction basins of coexisting states

In further numerical simulations we studied the sensitivity of the system response with respect to a variation of initial conditions. At low (below 0.036) values of the conductance G_{LP} an oscillatory state of the gamma type was reached for all tested initial conditions. On the other end, at sufficiently large (above 2.28) values of G_{LP} the system appears to possess a unique attractor as well: now this is the limit cycle which corresponds to the theta regime. In between, the system is bistable.

For a case study we take the value $G_{LP} = 0.8$, well inside the range of this parameter where distinct oscillations of the theta type coexist with the theta-gamma rhythmic pattern. The system has been scanned on a grid of initial conditions for the variables v_i and u_i from -2 to 2: these ranges correspond to the maximal span of gamma and theta-gamma oscillations for pyramidal cells. The initial size of the mesh has been taken as 0.01×0.01 and has been refined whenever necessary in order to resolve the fine details. It turned out that the choice of eventual attractor depends mostly on the initial values of the membrane potential and membrane variable of the slow cells.

To illustrate graphically the shape of the boundary between the attraction basins in the 12-dimensional space of initial values, we choose two characteristic intersections of this boundary with coordinate planes. The first one (left panel of Fig. 9) is the plane upon which all coordinates except v_p (the voltage variable of the pyramidal cell) and u_{L_1} (the gating variable of the left slow cell) are set to zero. The plot shows two distinct regions of theta oscillations separated by a strip which belongs to the basin of the theta-gamma state. Both borderlines display rather mild variations. Notably, the initial value of u_{L_1} should be sufficiently large to excite the theta oscillation: the initial strong contrast between the OLM cells (recall that $u_{L_2} = 0$ upon this plane) would facilitate the onset of a large phase difference between them, required for the theta state.

The second coordinate plane corresponds to the case when only the voltage variables of the OLM cells are initially excited whereas the rest of the variables start from zero values. In this projection (right panel of Fig. 9), the shape of the

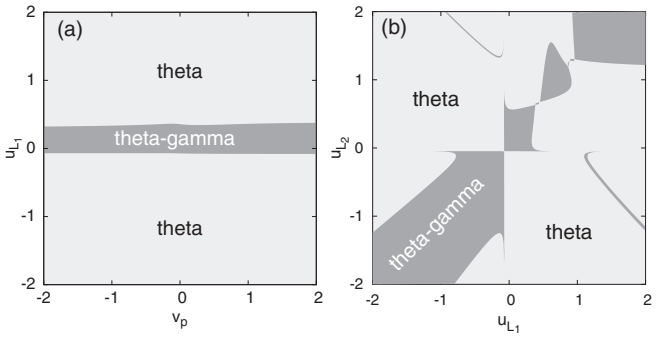

FIG. 9. Projections of attraction basins of coexisting rhythmic patterns. $G_{BL_1} = 0.06$, $G_{BL_2} = 0.03$, and $G_{LP} = 0.8$. Dark gray, attraction basin of the theta-gamma rhythm; Light gray, attraction basin of theta oscillations. (a) Initial values for the voltage of the pyramidal cell vs membrane variable of the left slow cell; the rest of the variables are set to zero. (b) Initial values for the membrane variables of two slow cells; the rest of the variables are set to zero.

attraction basins is much more intricate, with characteristic cusps, islands, and narrow bridges between them. Here again, we see that proximity between the initial states of the slow cells results, as a rule, in the eventual onset of the theta-gamma rhythmic pattern.

Experimentally relevant is the location of the border between the basins in terms of the membrane voltage of the slow cells. Numerics shows that this border (not presented graphically) looks quite simple: within the studied range of v_p there exists a threshold value of voltage $v_{L_{1,2}} \approx 0.14$ below which the unit oscillates in the theta-gamma rhythm whereas above it the theta rhythm has been registered.

F. Variation of asymmetry between *BL* synaptic connections

In order to elucidate the possible role of asymmetry in the pattern of synaptic connections, we performed calculations at different values of the ratio G_{BL_1}/G_{BL_2}. On decreasing this ratio from 2 to 1, we detected a qualitative distinction only at very low values of the conductance G_{LP}; otherwise, the results were largely similar to the ones described in the previous sections.

In the symmetric case $G_{BL_1} = G_{BL_2}$, the system possesses an invariant "diagonal" subspace in which the values of variables for the two slow cells coincide (hence, the phase shift between them is absent). Surprisingly, the states from this subspace are stable not only at moderate values of G_{LP} which correspond to an attractor of the theta-gamma type, but at low values of this parameter as well, where the temporal pattern belongs to the gamma type. In contrast to the previously described gamma oscillations, in this state the phase shift between the slow cells is absent; they oscillate in unison. Below we call this regime a "symmetric gamma state." If the conductance G_{LP} is set below 0.0016, the symmetric gamma oscillations are chaotic. Above this value of G_{LP} the periodic gamma state is observed; in a narrow interval close to $G_{LP} = 0.036$ its regular pattern is transformed (via the mixed mode) into the periodic theta-gamma oscillation. Outside the diagonal subspace there exists another,"asymmetric," oscillatory state which has the shape of gamma oscillations with a phase difference of $2\pi/3$ between the slow cells and is akin to the gamma state described in Sec. III A.

Accordingly, at sufficiently low values of G_{LP}, two qualitatively different types of gamma oscillations coexist: a symmetric one and an asymmetric one in which there is a phase lag between the slow cells. The asymmetric type, in its turn, consists of two different limit cycles: a state in which the phase of the cell L_1 is $2\pi/3$ ahead of L_2, as well as its mirror counterpart in which L_2 is "leading."

Depending on the initial conditions, the symmetrical network can display any of these three gamma patterns. Being structurally stable, all three limit cycles survive the introduction of weak asymmetry between the connections; of course, the former symmetric state develops in this case a small phase shift between the slow cells. Increase of G_{BL_1} at a constant value of G_{BL_2} initially results in the growth of the attraction basin of the oscillation with leading L_1 at the cost of the basins of two other gamma states. Further growth of G_{BL_1} brings about saddle-node bifurcations in which first the former symmetric gamma state and then the gamma state with leading L_2 disappear.

For example, at $G_{BL_2} = G_{LP} = 0.03$ all three gamma patterns coexist in the range of values of G_{BL_1} between 0.03 and 0.037 4. The saddle-node bifurcation of periodic orbits on the right border of this interval destroys the former symmetric pattern. Of the two remaining states with phase shift close to $2\pi/3$, the pattern with leading L_2 disappears in the saddle-node bifurcation at $G_{BL_1} = 0.047\,32$: beyond this value of G_{BL_1} only one pattern of the gamma type can be observed.

Let us return to characterization of the symmetric network with $G_{BL_1} = G_{BL_2} = 0.03$. Except for the "unison" symmetric gamma state, the appearance and properties of the gamma and theta oscillations display only small quantitative differences from the case $G_{BL_1} \neq G_{BL_2}$ described in the preceding sections. Two paragraphs above we have characterized solutions which at low values of G_{LP} look like a gamma oscillation with a phase shift between the slow cells close to $2\pi/3$. At around $G_{LP} = 0.073$ this pattern is rapidly transformed (via the mixed-mode oscillation) into the theta rhythm in which the slow cells oscillate in antiphase; stable theta oscillations persist in the whole studied range $G_{LP} \leqslant 3$. Similarly to the asymmetric case, at sufficiently high values of the conductance G_{LP}, the theta-gamma state has not been observed, and the theta oscillations are the only attractor of the system (cf. Fig. 6). In the absence of symmetry between $BL_{1,2}$, the periodic theta-gamma state is eliminated in the course of the saddle-node bifurcation. In the symmetric case, this bifurcation is replaced by the inverse pitchfork bifurcation; for $G_{BL_1} = G_{BL_2} = 0.03$ this event takes place at $G_{LP} = 2.014$. As a result, the periodic solution of theta-gamma type persists at higher values of G_{LP} as well, but is attracting only in the invariant "diagonal" subspace $u_{L_1} = u_{L_2}$ and $v_{L_1} = v_{L_2}$. A weak violation of the symmetry in initial conditions leads to creation and growth of a phase shift between the slow cells, which eventually destroys the theta-gamma oscillations and replaces them by the theta rhythm.

Concerning the border between attraction basins in the case of hysteresis between theta and theta-gamma rhythms, merely a quantitative shift due to variation of the ratio G_{BL_1}/G_{BL_2} has been observed; the shape of the basins is largely preserved.

Compared to Fig. 9(a), in the symmetric case $G_{BL_1} = G_{BL_2}$ the attraction basin of the theta-gamma state is slightly broader. In contrast, projection of attraction basins for the membrane variables of two slow cells [the analog of Fig. 9(b), which is symmetric with respect to the diagonal] displays a slight narrowing of the theta-gamma region. In addition, we have observed that symmetry in the conductances $G_{BL_{1,2}}$ lowers the threshold values of the membrane potentials $v_{L_{1,2}}$, which are necessary for the onset of the theta rhythm.

IV. DISCUSSION

In the preceding sections we have presented a minimalistic model for a working unit of the neuronal network in the hippocampus. Below we briefly discuss a few important aspects of this model.

A. Minimality of the network

Arguably, the size of the ensemble cannot be further reduced without introducing drastic distortions into the collective dynamics. For example, the omission of one of the slow L cells would disable the theta rhythm. As seen in Fig. 5, in this regime two L cells are oscillating in antiphase, and the fast pyramidal cell exhibits two spikes within a complete oscillation cycle: one spike comes shortly before the maximum of L_1 and the other one precedes the maximum of L_2. As soon as one slow partner is removed, this rhythmic pattern becomes impossible.

Further, our numerical experiments show that if the basket cell is removed from the configuration, the rhythmic patterns persist but their dependence on the strength of the coupling between the remaining pyramidal cell and the slow cells is weakened. If the configuration of connections is symmetric, the system is restricted to only one scenario of the onset of rhythms, which is mostly determined by the choice of initial conditions. This seems to contradict the experimental evidence which confirms that switching between the regimes depends on the coupling strength [7]. In the attempts to counteract the removal of the basket cell by asymmetry in the connections *from* the pyramidal cell *to* OLM cells, we observed that the region of existence of the theta-gamma regime is significantly reduced. Thus, we suppose that the presence of the basket cell allows the neuronal network not only to "maneuver" between different scenarios of emergence of all rhythms but also to expand the region of existence of the theta-gamma regime.

The role of asymmetry in this context is twofold. On the one hand, as shown in Sec. III F, the symmetric case possesses more attractors, which enhances the flexibility of the network. On the other hand, the reduction of variability in the strongly asymmetric network means an increase in the robustness, which can also be useful in certain situations.

B. Possible implications for larger networks

We started this section by defending our choice of the minimal model. Here we turn to the "inverse" question: are patterns, generated by this minimal unit, recognizable on the background of large hippocampal networks? Numerous experiments in the hippocampal areas CA1 and CA3 unambiguously confirm the existence of all the described oscillatory states: the gamma, the theta, and the theta-gamma [3,6,7]. Furthermore, the *in vitro* technique of taking directional cross sections in the hippocampus has allowed the patterns to be singled out: in longitudinal sections mostly the theta rhythm is recovered, whereas oscillations of gamma and theta-gamma type are typical for transverse and "medium" (so-called coronal) slices. This has to do with the morphology of the participating cells. The OLM cells are arborized (possess dendritic structure) mostly in the longitudinal direction. In longitudinal slices synaptic connections from these cells to the pyramidal and basket ones are at their strongest; this results in the synchronous theta rhythm in the area CA3 [6,7,29]. In other directions arborization is much less pronounced; hence, the relative role of the OLM cells is weaker, and one observes mostly the gamma and theta-gamma oscillations produced by interaction of pyramidal and basket cells.

Other kinds of cell contribute to the shaping and maintenance of rhythmic patterns as well: the study [10] lists at least 21 classes of inhibitory interneurons which participate in the oscillations. Any one of them could be a part of the minimal module. However, high synchrony among the inhibitory interneurons responsible for the gamma rhythm [5,6] allows one to restrict modeling to just one type: we have chosen the basket cells, whose interactions with pyramidal cells are well investigated experimentally. On adding the OLM cells which are required for the generation of the theta state, we get by with just three types of cell in a module.

How do such "modules" interact with each other in a large-scale network? What cells mediate the interactions? Which type of connection—excitatory or inhibitory—should be considered? From the point of view of morphological properties, briefly sketched above, it seems plausible that modules communicate with each other through OLM cells. The pyramidal and basket cells have been shown to be involved mostly in locally synchronized gamma oscillations [6]. Within this conjecture, the OLM cells of a module can inhibit pyramidal cells in the neighboring modules [29]. As for interactions between OLM and basket cells in large networks, reliable experimental data are still missing.

Spatial-temporal patterns in big networks depend on the strength of the connections between modules. For the case of strong coupling there is experimental evidence of phase theta waves [30]. In contrast, moderate coupling leads to spatial-temporal gamma oscillations which modulate slow theta patterns (clusters) [31]. Notably, such patterns are sensitive to the phase shift between the OLM cells. Finally, if the interaction is sufficiently weak, the modules oscillate independently of each other. In this case, rhythms found in a single module persist, and the presence of neighbors results, mostly, in shifting the transitions between them.

C. Multistability

Hysteretic properties, akin to the described effect of multistability, have been registered in experiments with subthalamic neurons [13]. In these experiments the application of different bias currents and shifting of the baseline membrane potential resulted in the onset of such different regimes as tonic firing, rhythmic bursts, or silent upstates. According to

the experimentalists, multistability can be controlled by the dynamics of ionic channels [13].

In our model, depolarization of the initial membrane potential of L cells results in the onset of the theta-gamma regime, but stronger depolarization switches the latter to pure theta oscillations.

To our knowledge, multistability of the discussed kind has not yet been registered in CA3, either in experiments or in existing theories. (The metastable states in large sections of CA3, experimentally found in Ref. [14], refer to alternating activity of different groups of neurons, and not to different rhythmic patterns.) In particular, the authors of the more detailed model described in Ref. [7] do not report on the coexistence of attractors. Transitions between rhythms can be related to the physiological state of a cell. The OLM cells are known to possess two specific ionic currents responsible for the onset of the theta rhythm [7,32]. One of these currents is activated by strong hyperpolarization, whereas the latter, in turn, is switched on by depolarization. These states correspond, respectively, to the top and bottom stripes in the left panel of Fig. 9; therefore in the corresponding ranges of potentials the theta regime is established. For the initial conditions from the "middle" stripe these currents are modest; hence the theta rhythm cannot develop, and the theta-gamma rhythm is observed instead. This interpretation requires, of course, an experimental testing.

ACKNOWLEDGMENTS

The authors are grateful to T. Gloveli, A. Ponomarenko, H. Rotstein, and S. Schreiber for fruitful and stimulating discussions. The research of A.L. and L.S.-G. was supported by the Bernstein Center, Berlin (Project No. A3) and BMBF (FKZ 01GQ1001A) and that of M.Z. by the DFG Research Center MATHEON (Project No. D21).

[1] A. T. Winfree, *The Geometry of Biological Time* (Springer, New York, 1980).
[2] J. O'Keefe and M. L. Recce, Hippocampus **3**, 317 (1993).
[3] G. Buzsaki, Neuron **33**, 325 (2002).
[4] K. D. Harris, J. Csicsvari, H. Hirase, G. Dragoi, and G. Buzsaki, Nature (London) **424**, 552 (2003).
[5] N. Hajos and O. Paulsen, Neuronal Networks **22**, 1113 (2009).
[6] T. Gloveli, T. Dugladze, S. Saha, H. Monyer, U. Heinemann, R. D. Traub, M. A. Whittington, and E. H. Buhl, J. Physiol. **562**, 131 (2005).
[7] T. Gloveli, T. Dugladze, H. G. Rotstein, R. D. Traub, H. Monyer, U. Heinemann, M. A. Whittington, and N. J. Kopell, Proc. Natl. Acad. Sci. USA **102**, 13295 (2005).
[8] G. Maccaferri and G. J. McBain, J. Physiol. **497**, 119 (1996).
[9] E. O. Mann, C. A. Radcliffe, and O. Paulsen, J. Physiol. **562**, 55 (2005).
[10] T. Klausberger and P. Somogyi, Science **321**, 53 (2008).
[11] F. Froehlich, T. J. Sejnowski, and M. Bazhenov, J. Neurosci. **30**, 10734 (2010).
[12] D. Durstewitz, Neuronal Networks **22**, 1189 (2009).
[13] J. I. Kass and I. M. Mintz, Proc. Natl. Acad. Sci. USA **103**, 183 (2006).
[14] T. Sasaki, N. Matsuki, and Y. Ikegaya, J. Neurosci. **27**, 517 (2007).
[15] P. Hahn and D. M. Durand, J. Comput. Neurosci. **11**, 5 (2001).
[16] P. Andersen, *The Hippocampus Book* (Oxford University Press, Oxford, 2007).
[17] N. Kopell, C. Borgers, D. Pervouchine, P. Malerba, and A. Tort, in *Hippocampal Microcircuits: A Computational Modeller's Resource Book*, edited by V. Cutsuridis, B. P. Graham, S. Cobb, and I. Vida, Chap. 15 (Springer, Berlin, 2010).
[18] P. J. Siekmeier, Behav. Brain Res. **200**, 220 (2009).
[19] F. Fröhlich and M. Bazhenov, Phys. Rev. E **74**, 031922 (2006).
[20] M. Rabinovich, R. Huerta, M. Bazhenov, A. K. Kozlov, and H. D. I. Abarbanel, Phys. Rev. E **58**, 6418 (1998).
[21] R. D. Traub, A. Bibbig, F. E. N. LeBeau, E. H. Buhl, and M. A. Whittington, Annu. Rev. Neurosci. **27**, 247 (2004).
[22] B. H. Singer, M. Derchansky, P. L. Carlen, and M. Zochowski, Phys. Rev. E **73**, 021910 (2006).
[23] H. D. I. Abarbanel, S. S. Talathi, L. Gibb, and M. I. Rabinovich, Phys. Rev. E **72**, 031914 (2005).
[24] M. A. Zaks, X. Sailer, L. Schimansky-Geier, and A. Neiman, Chaos **15**, 026117 (2005).
[25] D. Hennig and L. Schimansky-Geier, Physica A **387**, 967 (2008).
[26] R. FitzHugh, in *Biological Engineering*, edited by H. P. Schwan, Chap. 1 (McGraw-Hill, New York, 1969), p. 1.
[27] M. J. Gilles, R. D. Traub, F. N. LeBeau, C. H. Davies, T. Gloveli, E. H. Buhl, and M. A. Whittington, J. Physiol. **543**, 779 (2002).
[28] *Mixed Mode Oscillations: Experiment, Computation, and Analysis*, edited by M. Brons, T. J. Kaper, and H. G. Rotstein, focus issue of Chaos 18 (2008).
[29] A. Tort, H. G. Rotstein, T. Dugladze, and T. Gloveli, Proc. Natl. Acad. Sci. USA **104**, 13490 (2007).
[30] E. V. Lubenov and A. S. Siapas, Nature (London) **459**, 534 (2009).
[31] M. A. Belluscio, K. Mizuseki, R. Schmidt, R. Kempter, and G. Buzsaki, J. Neurosci. **32**, 423 (2012).
[32] F. Saraga, C. P. Wu, L. Zhang, and F. K. Skinner, J. Physiol. **552**, 673 (2003).